The Ancient Phosphatidylinositol 3-Kinase Signaling System Is a Master Regulator of Energy and Carbon Metabolism in Algae[1][OPEN]

Rishiram Ramanan,[a,b,2] Quynh-Giao Tran,[b,c,2] Dae-Hyun Cho,[b] Jae-Eun Jung,[d] Byung-Hyuk Kim,[b] Sang-Yoon Shin,[b,c] Sae-Hae Choi,[b] Kwang-Hyeon Liu,[e] Dae-Soo Kim,[d] Seon-Jin Lee,[f] José L. Crespo,[g] Hee-Gu Lee,[f] Hee-Mock Oh,[b,c] and Hee-Sik Kim[b,c,3]

[a]Department of Environmental Science, School of Earth Science Systems, Central University of Kerala, Tejaswini Hills, Periya, Kasaragod 671316, Kerala, India
[b]Cell Factory Research Center, Korea Research Institute of Bioscience and Biotechnology (KRIBB), Yuseong-gu, Daejeon 34141, Republic of Korea
[c]Department of Environmental Biotechnology, KRIBB School of Biotechnology, Korea University of Science and Technology, Yuseong-gu, Daejeon 34141, Republic of Korea
[d]Genome Research Center, KRIBB, Yuseong-gu, Daejeon 34141, Republic of Korea
[e]College of Pharmacy, Kyungpook National University, Daegu 41566, Republic of Korea
[f]Biomedical Genomics Research Center, KRIBB, Yuseong-gu, Daejeon 34141, Republic of Korea
[g]Instituto de Bioquimica Vegetal y Fotosintesis, Consejo Superior de Investigaciones Cientificas, Universidad de Sevilla, Seville 41092, Spain

ORCID IDs: 0000-0002-4641-9603 (R.R.); 0000-0001-5179-4603 (J.J.); 0000-0002-3285-5594 (K.L.); 0000-0003-3514-1025 (J.L.C.); 0000-0002-2151-3687 (H.O.); 0000-0002-9500-5394 (H.K.)

Algae undergo a complete metabolic transformation under stress by arresting cell growth, inducing autophagy and hyper-accumulating biofuel precursors such as triacylglycerols and starch. However, the regulatory mechanisms behind this stress-induced transformation are still unclear. Here, we use biochemical, mutational, and "omics" approaches to demonstrate that PI3K signaling mediates the homeostasis of energy molecules and influences carbon metabolism in algae. In *Chlamydomonas reinhardtii*, the inhibition and knockdown (KD) of algal class III PI3K led to significantly decreased cell growth, altered cell morphology, and higher lipid and starch contents. Lipid profiling of wild-type and PI3K KD lines showed significantly reduced membrane lipid breakdown under nitrogen starvation (−N) in the KD. RNA-seq and network analyses showed that under −N conditions, the KD line carried out lipogenesis rather than lipid hydrolysis by initiating de novo fatty acid biosynthesis, which was supported by tricarboxylic acid cycle down-regulation and via acetyl-CoA synthesis from glycolysis. Remarkably, autophagic responses did not have primacy over inositide signaling in algae, unlike in mammals and vascular plants. The mutant displayed a fundamental shift in intracellular energy flux, analogous to that in tumor cells. The high free fatty acid levels and reduced mitochondrial ATP generation led to decreased cell viability. These results indicate that the PI3K signal transduction pathway is the metabolic gatekeeper restraining biofuel yields, thus maintaining fitness and viability under stress in algae. This study demonstrates the existence of homeostasis between starch and lipid synthesis controlled by lipid signaling in algae and expands our understanding of such processes, with biotechnological and evolutionary implications.

Chlamydomonas reinhardtii, which possesses both animal and plant characteristics, has emerged as a model alga for studying lipid metabolism, flagellar assembly, photosynthesis, and other cellular processes (Merchant et al., 2007). Nutrient starvation in *C. reinhardtii* and other model algae leads to the synthesis of triacylglycerols (TAGs) by inducing membrane lipid hydrolysis and starch synthesis (Hu et al., 2008; Schmollinger et al., 2014; Kajikawa et al., 2015). The membrane lipid hydrolysis is mediated by lipases that release acyl-CoA from membrane lipids because these substrates are incorporated into the glycerol backbone of TAGs, which form the inner core of lipid droplets. There are several lipases in *C. reinhardtii* that efficiently catalyze this conversion (Li et al., 2012; Yoon et al., 2012).

In plant vegetative tissues, the breakdown of membrane lipids to TAGs under stress conditions is supposed to circumvent the harmful effects of free fatty acid (FFA) and reactive oxygen species (ROS) accumulation (Chapman et al., 2012; Hou et al., 2016). TAGs in mammalian tissues constantly accumulate and are recycled to FFAs based on a complex signaling network involving insulin (Wymann and Schneiter, 2008; Nemazanyy et al., 2015). On the other hand, it has been proved that inositide signaling inhibits Akt, a Ser/Thr kinase that in turn regulates Glc homeostasis and protein translation, thereby affecting insulin signaling growth (Chakraborty et al., 2010). In fact, several studies have demonstrated the major role of lipid signaling in growth, carbon metabolism, autophagy, apoptosis, and disease in mammalian models (Wymann and

Schneiter, 2008; Vanhaesebroeck et al., 2012; Shanware et al., 2013; Nemazanyy et al., 2015). Although it is widely known that algae hydrolyze membrane lipids similar to plants and homeostasis exists between TAG and membrane lipid hydrolysis, a definite mechanism has not been elucidated (Trentacoste et al., 2013). Moreover, the roles of algal lipid signaling and regulation in stress-induced responses are largely unexplored, although such mechanisms are known to occur in mammalian and plant models (Wymann and Schneiter, 2008; Couso et al., 2016; Hou et al., 2016). Algae are unique eukaryotes, as they produce both starch and lipid droplets as a response to any stress or starvation condition, linking plants and animals (Merchant et al., 2007). Therefore, algae are excellent model organisms for studying signaling and interactions between FFA, TAG, membrane lipids, and starch synthesis (Boss and Im, 2012; Vanhaesebroeck et al., 2012; Shanware et al., 2013).

Algae are considered to be a renewable feedstock for various bioproducts, including biofuels (Wijffels and Barbosa, 2010). Commercialization of algal biofuels has several bottlenecks, including current fossil fuel prices, high biofuel production costs owing to inadequate yields, and harvest inefficiencies. The most significant technical challenge in algal biofuel production is the trade-off between growth and accumulation of biofuel precursors, leading to modest yield. TAG and starch granules are precursors of biodiesel and bioethanol, respectively (Sheehan et al., 1998; Hu et al., 2008; Wijffels and Barbosa, 2010; Merchant et al., 2012). Even after several decades of research in this area, the molecular mechanism for this dichotomy is still unresolved (Sheehan et al., 1998). Therefore, studying the signaling mechanism behind growth, starvation, and starvation-related responses is critical to the success of algal biofuels.

Phosphatidylinositol 3-kinase (PI3K) signaling in higher eukaryotes has been connected to starvation-induced processes, including autophagy, lipid metabolism, and cell survival (Boss and Im, 2012; Chapman et al., 2012; Vanhaesebroeck et al., 2012; Shanware et al., 2013). PI3K is also known to have a major role in insulin-dependent Glc homeostasis in higher eukaryotes (Nemazanyy et al., 2015). Class III PI3K enzyme is the oldest class of this enzyme present in all known eukaryotes and is the only class in algae, yeasts, and plants (Vanhaesebroeck et al., 2012). Moreover, phosphatidylinositol 3-phosphate (PI3P) is thought to be the first known phosphatidylinositol lipid to appear during evolution, having been found in both bacteria and archaea (Irvine, 2016). Earlier studies on PI3K in *C. reinhardtii* have shown that the protein is encoded by a single copy gene, *Vacuolar protein sorting34* (*VPS34*; Molendijk and Irvine, 1998). It has been speculated that PI3P may act as a signaling molecule based on its rapid turnover in pulse-chase experiments in *Chlamydomonas eugematos* and that PI3K in algae may act as a signaling system (Irvine et al., 1992; Munnik et al., 1994; Molendijk and Irvine, 1998). In addition, a recent study on inositide signaling in *C. reinhardtii* implicated the signaling network in nutrient sensing and starvation-triggered responses (Couso et al., 2016).

Here, we show that PI3K regulates the homeostasis of membrane lipids, TAGs, starch, FFA, and ATP by influencing other components of the signaling network. Hence, the PI3K signaling cascade independently influences the energy homeostasis. The PI3K KD lines also display significant differences in phenotype and genotype related to growth and lipid metabolism. PI3K is known to play a major role in autophagosome formation in higher eukaryotes (Shanware et al., 2013). The selected mutant line reveals autophagy induction under stress, thereby nullifying any role of selective autophagic processes in the observed phenotype. Therefore, this cascade in algae performs a plethora of functions critical for the survival and fitness of the organism, especially in an oligotrophic environment. From a biofuel perspective, this study sheds light on the regulatory mechanisms behind the tradeoff between growth and biofuel precursor accumulation. Our findings demonstrate that signal transduction pathways might provide vital clues to several outstanding research bottlenecks in algae and that engineering signaling pathways might be one way forward.

RESULTS

Inhibition and Knockdown of Class III PI3K Increases Lipid and Starch Contents in Algae

The green algal PI3K protein encoded by the *VPS34* gene is highly conserved and is more closely associated with homologs from higher plants than other protists and mammals, which suggests conservation in green lineage (green algae and land plants; Fig. 1A; Finet et al., 2010; Mikami, 2014). The *C. reinhardtii* PI3K is an extraordinarily large 125-kD protein with a novel insert region in the N terminus of the catalytic domain

[1]This work was supported by a grant from the host institution through the Korea Research Institute of Bioscience and Biotechnology (KRIBB) Research Initiative Program (www.kribb.re.kr), the Advanced Biomass R&D Center of the Global Frontier Project funded by the Ministry of Science, ICT and Future Planning (2015M3A6A2065697), and a grant from the Marine Biotechnology Program funded by the Ministry of Oceans and Fisheries (20150184).

[2]These authors contributed equally to the article.

[3]Address correspondence to hkim@kribb.re.kr

The author responsible for distribution of materials integral to the findings presented in this article in accordance with the policy described in the Instructions for Authors (www.plantphysiol.org) is: Hee-Sik Kim (hkim@kribb.re.kr).

R.R. and H.-S.K. designed the study; R.R., Q.-G.T., S.-Y.S., B.-H.K., K.-H.L., and S.-H.C. conducted experiments; R.R., D.-H.C., J.-E.J., D.-S.K., S.-J.L., J.L.C., K.-H.L., Q.-G.T., and H.-S.K. analyzed the data; R.R., H.-G.L., H.-M.O., J.L.C., and H.-S.K. wrote the manuscript with the contribution of all authors.

[OPEN]Articles can be viewed without a subscription.

www.plantphysiol.org/cgi/doi/10.1104/pp.17.01780

(Molendijk and Irvine, 1998). PI3K is known to be associated with starvation-related responses and lipid metabolism in higher eukaryotes (Boss and Im, 2012; Chapman et al., 2012; Vanhaesebroeck et al., 2012; Shanware et al., 2013). Therefore, we tested the related phenotypic responses of *C. reinhardtii* after treatment with different PI3K inhibitors. Significantly enhanced TAG fluorescence was observed in *C. reinhardtii* cc124 (wild type) upon PI3K inhibition with 3-methyladenine (3MA) and wortmannin, especially under nitrogen (N) starvation (Supplemental Fig. S1). Further studies with 3MA showed that PI3K inhibition also increased lipid content in wild type under N-sufficient (+N, 9 d, unless otherwise mentioned) and acute starvation (–N, 48 h, unless otherwise mentioned) conditions (Supplemental Fig. S1). Similarly, 3MA treatment in *Scenedesmus obliquus* also resulted in increased TAG, confirming our initial hypothesis that PI3K has a critical role in regulating lipid metabolism in algae like in higher eukaryotes (Supplemental Fig. S1). Therefore, PI3K knockdown (KD) *C. reinhardtii* mutants were generated to further study the role of PI3K in lipid signaling in algae.

C. reinhardtii KD lines displayed similar morphological characteristics compared to wild-type and mock (empty vector) lines. The KD mutants had reduced growth particularly in photoautotrophic conditions, in the presence and absence of N (Fig. 1B). Most PI3K KD lines showed increased total lipid content, especially in –N conditions, increased TAG content, and increased cell size compared to both the mock and wild-type lines. KD lines were also more circular in shape compared to wild-type and mock lines and displayed an inability to move in +N conditions (Supplemental Fig. S2; Supplemental Data Set 1). Among the three KD lines, T1B3 and T411 lines showed altered growth patterns (Fig. 1C), while the T411 line showed severely impaired growth under both mixotrophic and photoautotrophic conditions in both +N and –N conditions. Principal component analysis (PCA) of the above morphological, physiological, and genotypic traits of the mutants showed that all KD lines clustered together, whereas wild-type and mock lines clustered separately. It must be noted that KD lines under +N and –N conditions clustered separately, whereas wild-type and mock lines clustered together even though the conditions differed. T1B3 and T411 lines displayed significantly decreased *VPS34* transcript levels ($P \leq 0.05$) compared to the mock and wild-type lines (Supplemental Fig. S2, E and F) under +N and –N conditions. Although both T1B3 and T411 lines had similar phenotypic, physiological, and genotypic characteristics, confirming the knockdown of PI3K, the T411 line was selected for further studies due to its phenotypic stability across generations (Fig. 2). These studies confirmed that the T411 line consistently showed highly reduced cell growth in +N and –N conditions across generations and a milder green hue that was reinforced with decreased PI3P generation, confirming reduced PI3K enzyme activity ($P \leq 0.01$). However, there were no significant changes to protein and chlorophyll content in T411 in +N and –N conditions while the starch content increased significantly in T411, reaching 38% DCW in –N conditions (Fig. 2F).

Furthermore, the T411 line showed insignificant changes in TAG levels in +N and –N conditions (Fig. 3A). However, higher TAG fluorescence was observed under high-light stress conditions (Supplemental Fig. S3). Repeated efforts to knock down the *VPS34* gene in starchless mutants consistently resulted in lethal mutations. This result, taken together with reduced cell numbers in KD lines, shows that severe knockdown of PI3K would result in unviable mutants, possibly because of issues in cell division. These results indicate that substantial metabolic changes occur in the mutant related to growth and starch and lipid metabolism. Therefore, we performed additional lipidomics analyses in wild-type and T411 cells grown in +N and –N conditions.

PI3K Regulates Membrane Lipid Hydrolysis in N Starvation

Algal lipids were profiled using direct infusion nanoelectrospray-tandem mass spectrometry in both ionization modes. Twenty-nine lipid species (11 DGTS, 11 TAG, 4 Lyso-DGTS, and 3 DGDG) were identified in the positive-ion mode. Thirteen lipid species (5 PG, 4 SQDG, 3 MGDG, and 1 PI) were identified in the negative-ion mode (Supplemental Tables S1 and S2). The statistical analysis of algal lipid profiles showed a clear separation among all sample groups (WT+N, WT–N, T411+N, T411–N; $P < 0.001$; Supplemental Fig. S4, A and C). The levels of most membrane lipids except for MGDG were either significantly increased or did not show any significant change in T411+N cells compared to WT+N (Fig. 3B). The decrease in MGDG in both conditions in the T411 line is likely due to the role of MGDG as a precursor for acyl groups that are incorporated into TAGs via membrane lipid breakdown in *C. reinhardtii* (Li et al., 2012). Several membrane lipid species showed high levels in T411–N compared to WT–N conditions ($P \leq 0.01$). For example, the levels of membrane lipid species (DGTS 34:1, LysoDGTS 18:2, DGDG 34:3, SQDG 34:4, PI 34:1, PG 32:0 and PG 34:1) were higher in T411–N than in all other sample groups (Supplemental Table S2). Thus, these results indicate either arrested membrane lipid hydrolysis or continuous membrane lipid biosynthesis in PI3K KD cells. This result is unique, as all known algal model species degrade membrane lipids upon N starvation (Hu et al., 2008; Li et al., 2012). Of the 11 TAG species identified, one TAG (TAG 50:4) showed significantly decreased levels ($P \leq 0.05$) in T411, and the remaining TAGs showed no significant difference compared to wild type under N-replete conditions (Fig. 3). There was no significant change in the fatty acid (FA) composition of the mutant except for the increase in oleic acid and linoleic acid during starvation (Supplemental Fig. S4D). The findings of unaltered membrane lipid levels

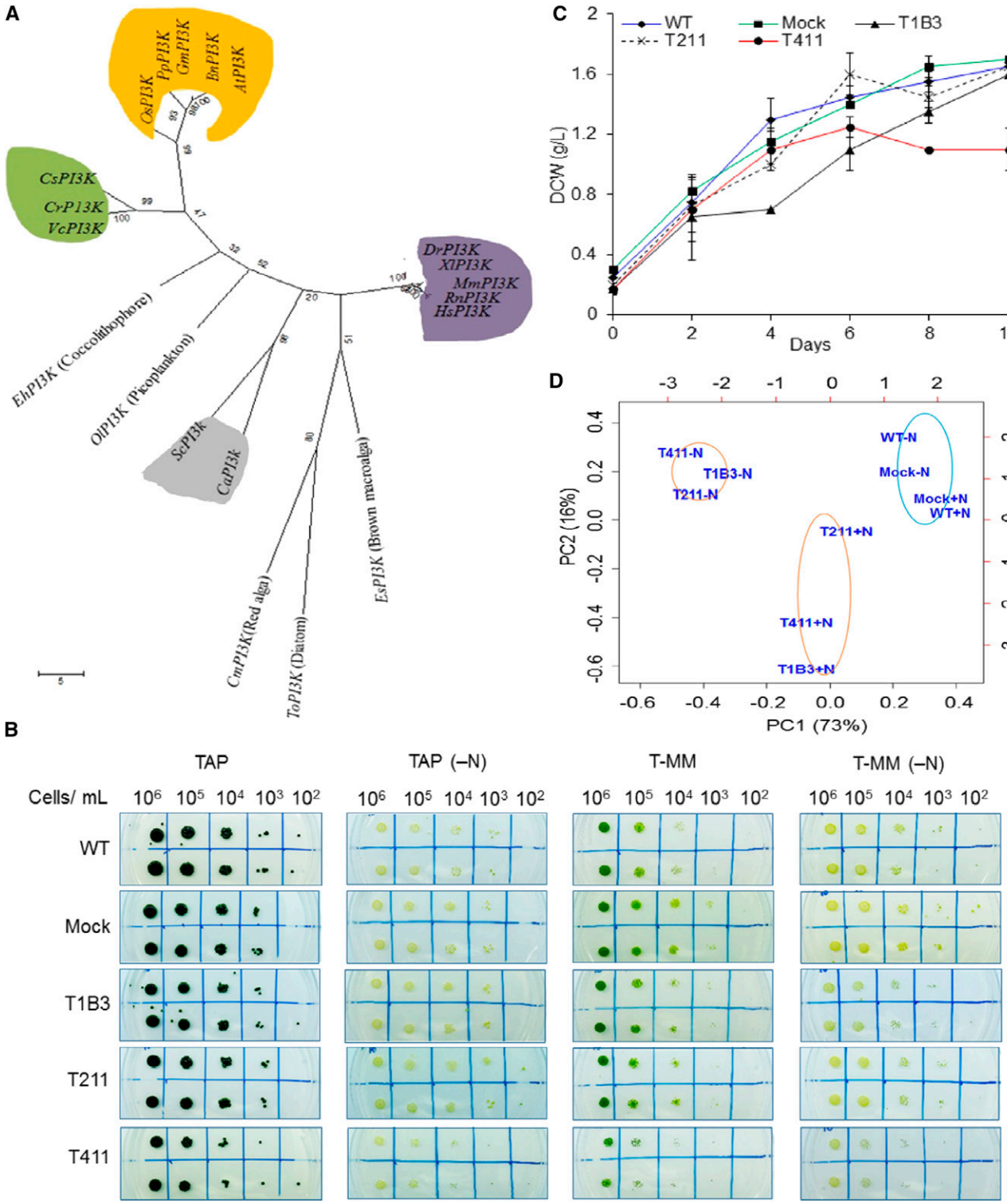

Figure 1. Phylogenetic analysis of class III PI3K enzymes from algae, plant, and animal kingdoms and screening of *VPS34* knockdown mutants through physiological analyses. A, Phylogenetic tree of class III PI3K using amino acid sequences from algae, plant, and animal kingdoms. The tree was constructed using a maximum parsimony method, and the bootstrap values (1,000 replicates) are shown on each node. Heterodimeric class III PI3K (vacuolar protein sorting 34, *VPS34*) of *C. reinhardtii* was clustered with other green algal homologs (green). PI3Ks from plants are clustered together (orange) and are closely related to green algae. The animal PI3Ks are clustered together (purple), fungi, yeast (gray), and other algal PI3Ks are not related to plant and animal PI3Ks and may have different origins. B, *C. reinhardtii* cc124 (wild type [WT]), the mock and the KD lines were grown in photoautrophic and mixotrophic conditions in the presence and absence of N. C, The growth pattern of wild type,

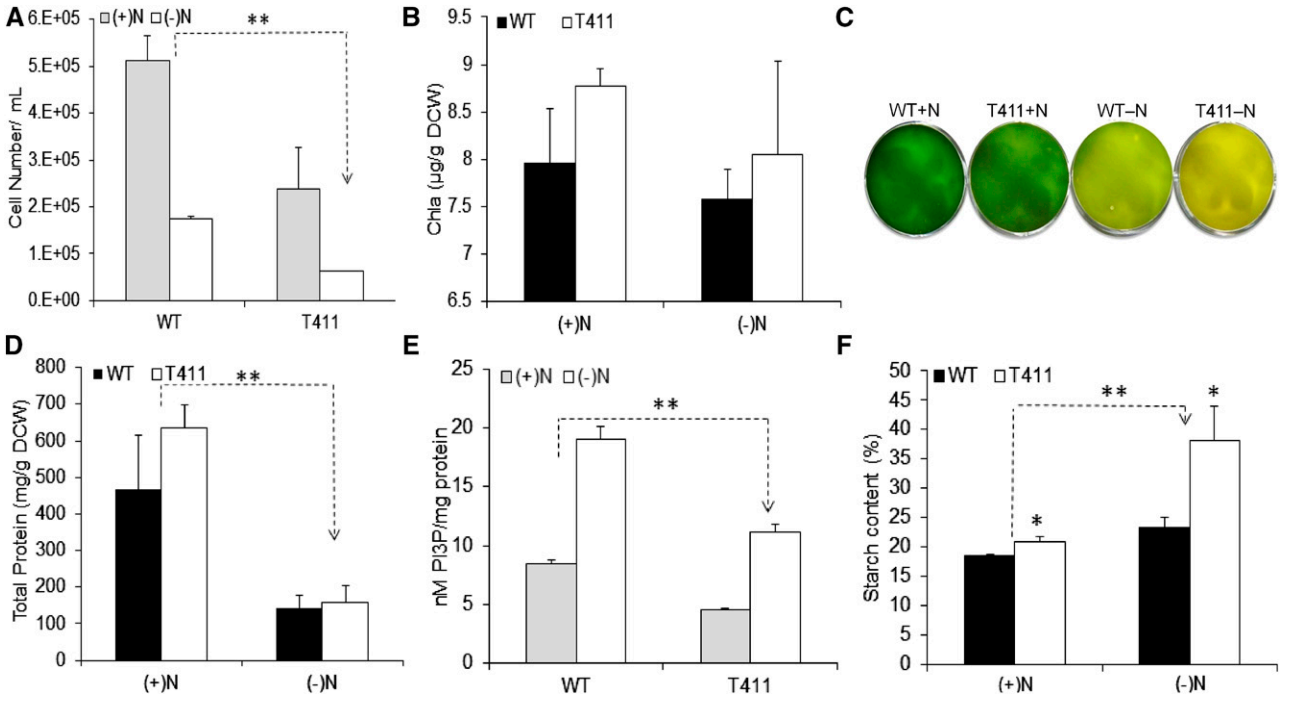

Figure 2. Comparison of wild-type and PI3K KD (T411) cell physiology. A, Number of wild-type (WT) and T411 cells in +N and –N conditions. There were significantly fewer T411 cells than WT cells ($P \leq 0.01$). B, The chlorophyll content of the wild-type and mutant in +N and –N conditions. Appearance of wild-type and mutant in +N and –N conditions, C. The total protein content of sample sets, and all sample sets exhibited significantly reduced protein content under –N growth conditions, D. The T411 line showed significantly decreased enzyme activity than the wild type in terms of phosphatidylinositol 3-phosphate (PI3P) production, E. The starch content of wild-type and T411 under acute starvation, F. All experimental analyses were performed with three biological replicates, and the mean ± SD value is presented. $^{**}P \leq 0.01$, $^{*}P \leq 0.05$. The *P* value was calculated using Student's *t* test and ANOVA.

except for MGDG and significantly higher TAG levels in T411–N compared to T411+N indicate that an alternative route for TAG synthesis manifested under stress in the T411 line. These changes in TAG synthesis and increased starch levels might radically alter cellular energy metabolism (Johnson and Alric, 2013). Therefore, global gene expression analysis of the sample groups was performed.

Rerouting of Carbon from Starch to TAGs via De Novo FA Biosynthesis

The RNA-seq analyses showed that more than 2,000 genes were differentially expressed in T411 compared to wild type in +N conditions (Fig. 4). There were an additional 1,000 genes differentially expressed in –N conditions (Fig. 4A). Previous transcriptomic studies in *C. reinhardtii* identified a systemic down-regulation of membrane lipid biosynthesis genes and up-regulation of various lipases following N depletion (Miller et al., 2010; Gargouri et al., 2015). The up-regulation of key genes involved in the biosynthesis of glycerophospholipids (*EPT1*, *BTA1*, and *PGP3*) and down-regulation of a majority of lipases, including putative TAG lipases and lysophospholipases, were observed in T411–N compared to WT–N (Fig. 4B). Additionally, all identified type 2 *DGAT* genes (*DGTT*) and the *PDAT* gene, which is involved in TAG synthesis, were consistently up-regulated in T411–N (Fig. 4C; Wymann and Schneiter, 2008). Among the phosphoinositol-signaling genes, *VPS34* and *PI4K* were downregulated in T411–N. Other key genes in the pathway (*PIS1* and phosphoinositol-specific *PLCD*), were upregulated (Fig. 4D; Boss and Im, 2012). These results indicate that TAG accumulated in T411 cells without assistance from membrane lipid turnover and substantiate earlier observations in physiological and lipid profiling analyses (Figs. 1–3; Supplemental Fig. S2). However, the source of carbon

Figure 1. (*Continued.*)
mock, and mutant lines. D, Principal component analyses (PCAs) of various morphological, physiological, and genetic analyses such as area and shape, total lipid content, TAG levels, and *VPS34* gene expression levels of the KD lines, mock, and wild type in both +N and –N conditions. The data used for PCA have been depicted in Supplemental Figure S2.

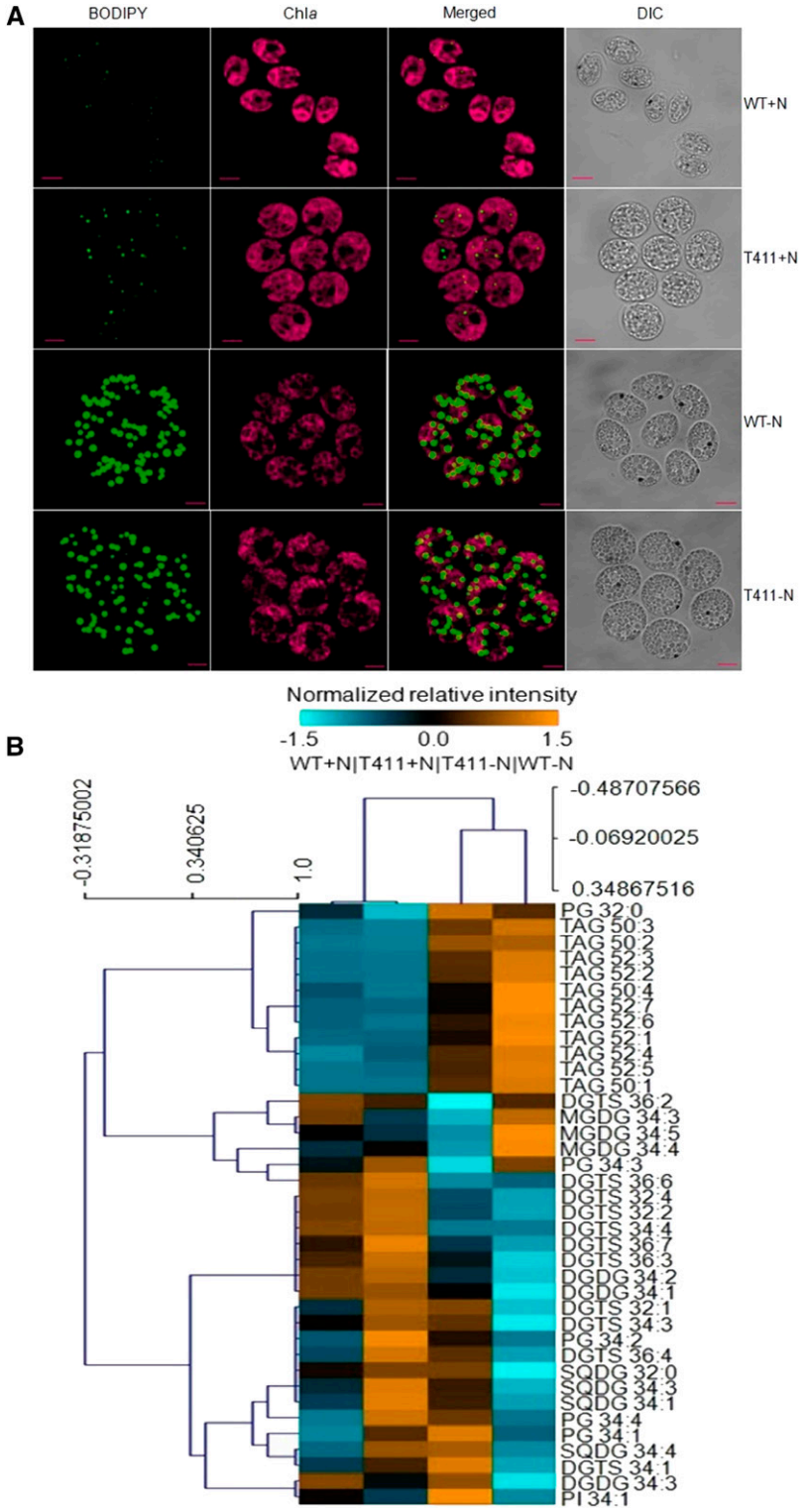

Figure 3. Imaging and lipidomic profiling of wild type and T411 under +N and −N conditions. A, Confocal imaging confirmed there were larger and more circular mutant cells that exhibited mildly higher TAG fluorescence in both conditions than the wild type (WT). The scale bar indicates 5 μm. B, The total lipids isolated from the wild type and T411 under +N and −N were subjected to Nanomate LTQ-MS/MS analysis. A heat map of 38 lipid species, excluding four lyso-DGTS species, were detected. DGTS, diacylglyceryltrimethylhomo-Ser; MGDG, monogalactosyldiacylglycerol; DGDG, digalactosyldiacylglycerol; SQDG, sulfoquinovosyldiacylglycerol; PI, phosphatidylinositol; PG, phosphatidylglycerol; TAG, triacylglycerol. The elemental compositions and proposed molecular formula are described in Supplemental Table S1. The precise intensity ratio values are presented in Supplemental Table S2.

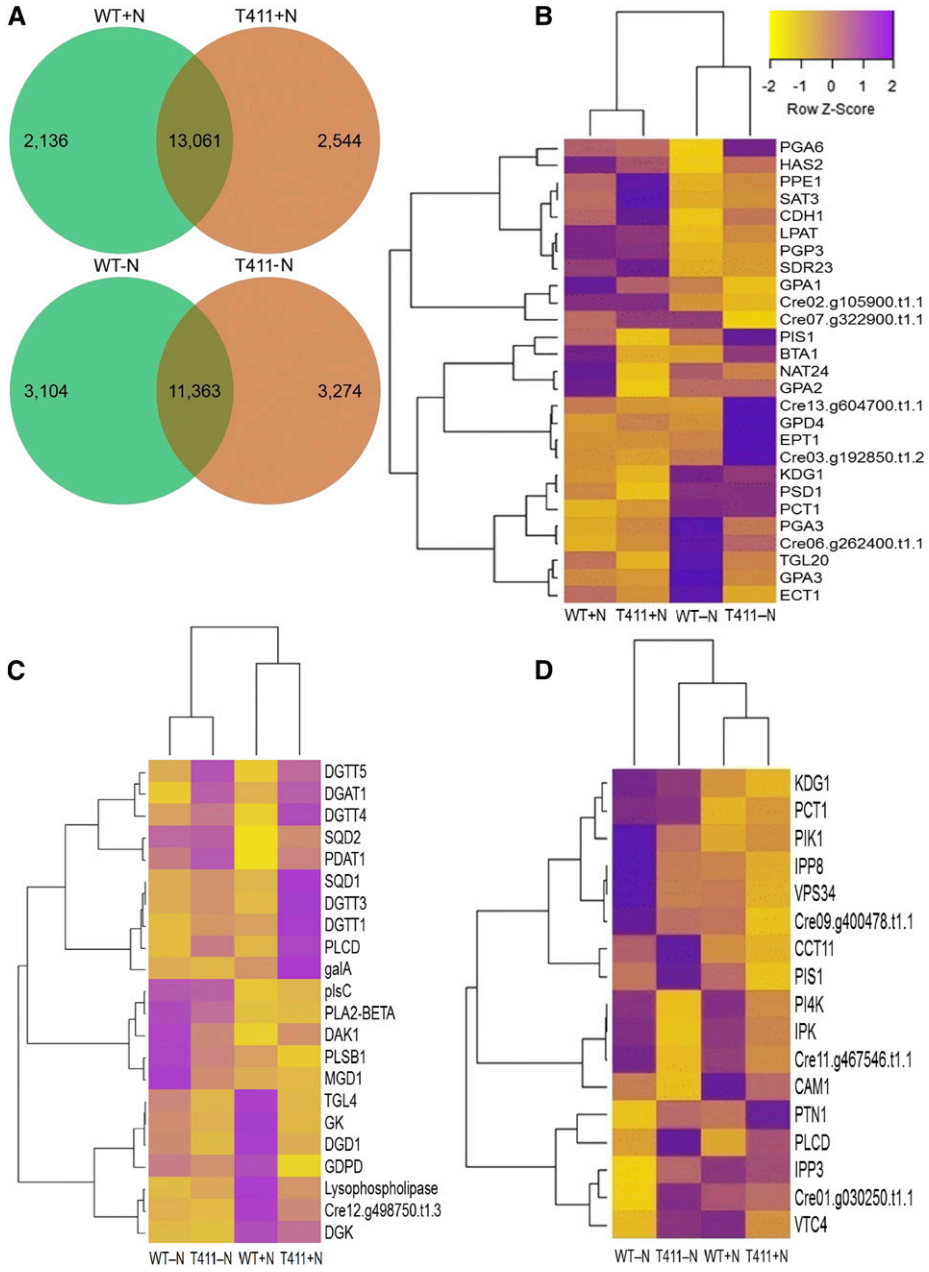

Figure 4. RNA-seq analysis of lipid metabolism and signaling pathways under growth and starvation conditions. A, Venn diagram showing overlapping transcripts among the total transcripts with ≥2-fold change in expression obtained from the wild type (WT) and T411 mRNA under +N and –N conditions. Heat map and cluster analysis of the differential gene expression of genes involved in the glycerophospholipid pathway, B, glycerolipid pathway, C, and PI signaling pathway, D, in wild-type and T411 cells under +N and –N conditions. For detailed gene annotation, please refer to Supplemental Table S5.

for TAG accumulation was unclear because the starch concentration in acute starvation condition was significantly higher in T411. Therefore, a gene network analysis was performed using the transcript data set to trace this differential route in the T411 line.

We selected four pathways for the gene expression network because related studies in *C. reinhardtii* suggested that under –N conditions, acetyl-CoA was directed toward the tricarboxylic acid (TCA) cycle for energy production and partly for FA synthesis (Johnson and Alric, 2013; Ramanan et al., 2013; Goodenough et al., 2014; Avidan et al., 2015; Gargouri et al., 2015). Starch is hydrolyzed through glycolysis to produce pyruvate after the initial accumulation stage, which eventually feeds into the TCA cycle (Gargouri et al., 2015). Similar results were obtained in wild-type cells in –N conditions, where starch accumulated and was subsequently hydrolyzed by glycolysis (Fig. 5). Genes

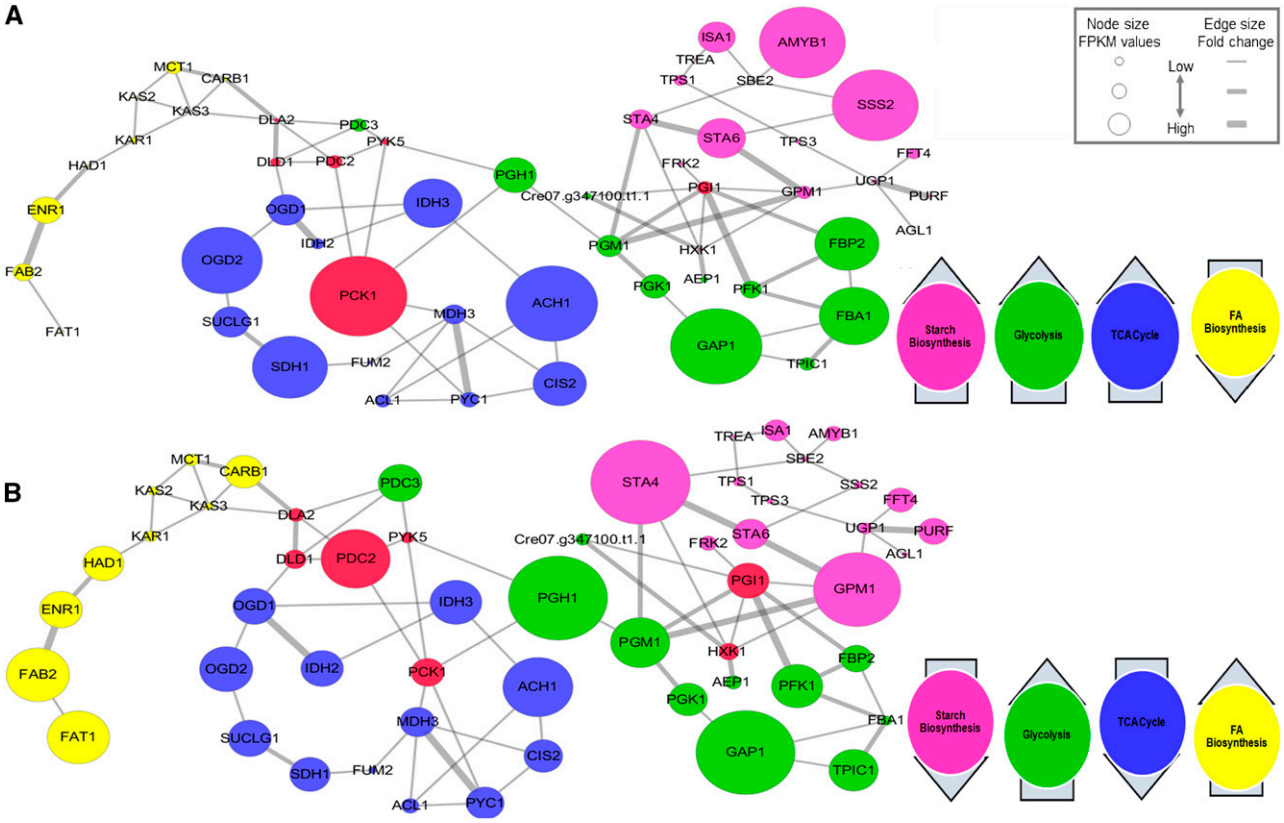

Figure 5. Gene network analysis of four pathways involved in energy metabolism under stress in algae. A, Gene network of the wild type (WT) under –N conditions based on the FPKM values compared to the wild type under +N conditions. The gene network was constructed using relative mRNA levels and was visualized by Cytoscape v 3.2.1. The circular edges represent FPKM values, and each node represents the relative fold change between adjoining edges. B, Gene network of T411 under –N conditions based on the FPKM values compared to the wild type under +N condition. Green circles represent glycolysis pathway genes; blue represents TCA pathway genes; pink represents starch and Suc metabolism pathway gene; yellow represents FA biosynthesis pathway genes; and red represents genes influencing more than one pathway. For detailed gene annotation, please refer to Supplemental Table S5.

encoding soluble starch synthases (*SSS* isoforms) and *STA6* were significantly upregulated in WT–N, which indicates increased starch accumulation compared to WT+N cells ($P \leq 0.01$; Fig. 5A). The glycolysis genes *GAP1*, *PGI1*, and *PFK1* were significantly upregulated ($P \leq 0.01$). Unexpectedly, the T411 line downregulated *SSS* isoforms and *STA6* transcripts compared to WT–N while *GAP1*, *PGI1*, *PFK1*, and *HXK1* were highly upregulated (Fig. 5B; $P \leq 0.01$). The key TCA genes, such as *CIS2* and *SDH1*, were highly upregulated in WT–N but downregulated in T411–N. The majority of FA biosynthesis genes were upregulated in T411–N compared to WT–N, including the *CARB1* gene, which catalyzes the first committing step in FA synthesis (Goodenough et al., 2014). The expression levels of some FA biosynthesis genes in T411–N were even higher than those in WT+N. Moreover, genes such as *GPD2*, which connects carbon assimilation and gluconeogenesis to TAG synthesis, showed a nineteen-fold increase in T411–N compared to WT–N.

These results suggest that acetyl-CoA generated from acetate in the medium was rerouted to FA biosynthesis under acute starvation conditions and bypassed the TCA cycle in the mutant. A relevant study on gene coexpression network based on RNA-seq data suggested that there is a definite nexus between carbon and nitrogen metabolism and signaling networks during starvation (Romero-Campero et al., 2016). The study directly connects TAG accumulation assisted by *PDAT* with phospholipid signaling in one of the central clusters. Although integrated omics and network analyses of PI3K KD established the nexus between signaling, growth, and metabolism and the regulation of membrane lipid turnover, several questions remained. For instance, the down-regulation of several starch biosynthesis genes in T411–N contrasted with the high starch levels noted in the mutant under acute starvation. Hence, starch levels under prolonged growth (21D+N, 21 d) and starvation conditions (15D–N, 15 d) were analyzed to further investigate this finding. Starch levels in the wild type and T411 cells were similar

in 21D+N (prolonged N replete growth, ~24%) and 15D–N (prolonged N starvation, ~36%), which differs from the results observed under the –N conditions. The lower starch levels in the mutant under prolonged starvation compared to acute starvation showed that starch was hydrolyzed, as seen in network analyses. Based on these results, we concluded that after acetate exhaustion under prolonged starvation (akin to photoautotrophic mode), starch was hydrolyzed through glycolysis to enable FFA biosynthesis in T411 cells (Fig. 5; Supplemental Fig. S4E; Johnson and Alric, 2013; Gargouri et al., 2015).

Increased FFA Production in T411 Reduces Survivability

We sought further confirmatory evidence of increased FFA biosynthesis in the mutant by analyzing FFA levels in acute and prolonged growth and starvation conditions in wild type and T411 (+N, –N, 21D+N, 15D–N; Fig. 6). The FFA levels in the mutant were higher in +N conditions and were significantly reduced under –N conditions ($P \leq 0.05$), in contrast to the observations in wild-type cells (Fig. 6A). The FFA levels under the 21D+N ($P \leq 0.05$) and 15D–N ($P \leq 0.01$) conditions were much higher than the wild-type levels, substantiating the up-regulation of FA biosynthesis genes in T411–N (Fig. 6B). These results indicate that the continuous production of FFA in T411 compensates for decreased acyl-chain accumulation following arrested lipid hydrolysis and drives TAG accumulation. The mutant uses the initial acetate available for FFA synthesis followed by TAG accumulation, which explains the reduced FFA levels under acute starvation. Eventually, after acetate exhaustion, the mutant continuously produces FFAs, akin to tumor cells. In mammalian models, it has been established that tumor cells have altered lipogenesis and lipolytic mechanisms compared to normal cells. In fact, activation of FA synthesis is critical for carcinogenesis (Zaidi et al., 2013). In précis, the PI3K KD showed divergence from membrane lipid breakdown, an essential stress response in plants and algae, and enhanced/uninhibited FFA synthesis, a proven trait of malignancy. Thus, algae may serve as a focal model for studying the evolution of lipid signaling in eukaryotes, linking plant and animal models (Merchant et al., 2007).

On the other hand, unlike malignant cells, T411 cells had retarded growth compared to wild type. Furthermore, analysis of transcriptomic responses of genes related to flagellar assembly also corroborated with phenotypic analyses that the mutant line was nonmotile as most genes were downregulated in the T411 line in both +N and –N conditions (Supplemental Fig. S5; Supplemental Data Set 1). Therefore, we postulated that the T411 cells used available energy for survival inefficiently. To test this hypothesis, the ATP levels in the wild-type and T411 cells in all conditions (+N, –N, 21D+N, 15D–N) were evaluated. The ATP levels under –N were higher in the wild-type cells ($P \leq 0.05$), and as previously reported, *C. reinhardtii* continues to actively generate ATP in mitochondria through the TCA cycle (Johnson et al., 2014). This increase may compensate for starvation and sustain essential cellular processes. Conversely, the ATP levels in T411–N were considerably lower than in WT–N ($P \leq 0.05$) and were slightly lower than in T411+N (Fig. 6C). The prolonged growth and starvation conditions further reduced ATP levels in T411 ($P \leq 0.01$; Fig. 6D).

PI3K Signaling Overrides Autophagic Responses in *C. reinhardtii*

Autophagy is another important aspect of class III PI3K signaling, contributing essential ATP under stress in all known eukaryotes (Shanware et al., 2013). Class III PI3K is actively involved in autophagosome formation and is essential for selective autophagic processes, such as lipophagy in mammals (Singh et al., 2009). Moreover, high starch phenotype has been associated with decreased autophagic flux in PI3K-silenced Arabidopsis (*Arabidopsis thaliana*; Wang et al., 2013). Autophagy is also activated in *C. reinhardtii* under stress conditions and in the presence of ROS (Pérez-Pérez et al., 2012). We analyzed the transcript abundance of *ATG* genes to investigate whether the T411 line has reduced autophagic activity, resulting in increased starch levels. Several genes involved in the autophagy process were down-regulated, including *Autophagy-related protein1* (*ATG1*) and *Vacuolar protein sorting15* (*VPS15*), which is a regulatory subunit of *VPS34* (Díaz-Troya et al., 2008). The *Autophagy-related protein8* (*ATG8*) gene did not show differential expression in either the RNA-seq or reverse transcription (RT)-PCR analyses (Supplemental Fig. S6, A and B). The immunoblot analysis of ATG8 protein showed increased lipidation of ATG8 in the mutant under +N conditions (Supplemental Fig. S6C). Although transcript abundance of many autophagy-associated genes decreased significantly, the ATG8 lipidation pattern suggests induction of autophagy under normal growth and starvation (Díaz-Troya et al., 2008; Pérez-Pérez et al., 2012; Wang et al., 2013). However, the gene target of rapamycin (*TOR1*) was upregulated, while *5′ AMP-activated protein kinase* (*AMPK*) was downregulated (Supplemental Fig. S6, A and B). Therefore, PI3K in *C. reinhardtii* might have a significant role in nutrient perception and signaling in association with *TOR1* and *AMPK* (Díaz-Troya et al., 2008; Hardie et al., 2012; Couso et al., 2016). The combination of PI3K and *AMPK* might have a major role in maintaining cellular ATP levels in *C. reinhardtii* because the T411 line had highly reduced ATP levels despite the induction of autophagy.

DISCUSSION

Our results suggest that PI3K-dependent autophagic processes have a relatively minor role in sustaining ATP levels under stress in *C. reinhardtii* (Díaz-Troya et al., 2008; Pérez-Pérez et al., 2010, 2012). Moreover,

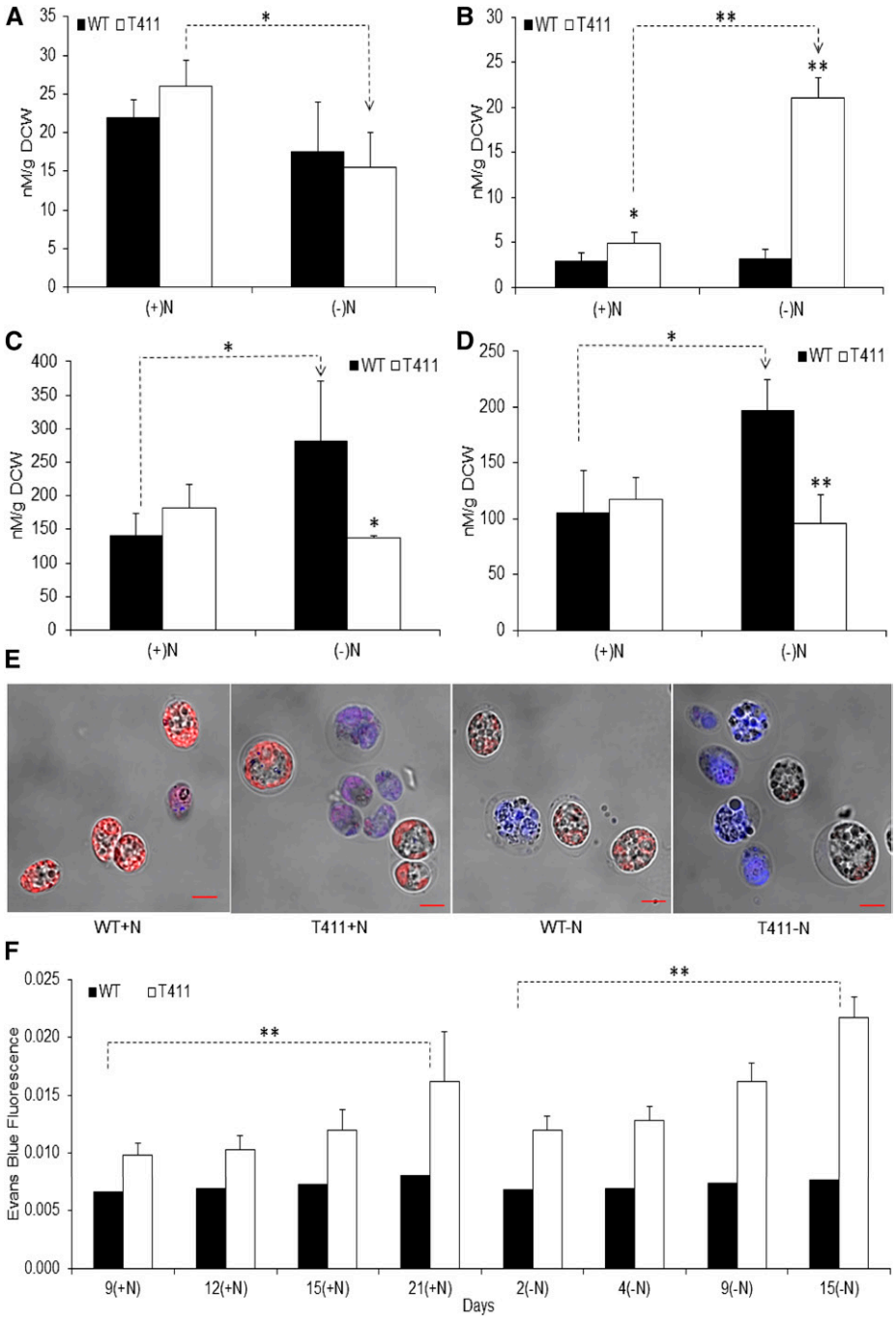

Figure 6. Energy levels and viability of wild type and T411 under different conditions. FFA levels in the wild type (WT) and T411 under the early stationary phase and acute starvation, A, and prolonged growth and starvation, B. ATP levels in the wild type and T411 under the early stationary phase and acute starvation, C, and prolonged growth and starvation, D. A confocal laser scanning microscopy merged image of Evans blue-stained wild type and T411 under prolonged growth and starvation conditions. The scale bar indicates 5 μm, E. Time-course analysis of the fluorescence intensity of the Evans blue viability stain measured by FACS in sample groups under both conditions, F. All experimental analyses were performed with three biological replicates, and the mean ± SD value is presented. $^{**}P \leq 0.01$, $^{*}P \leq 0.05$. The *P* value was calculated using Student's *t* test and ANOVA.

selective autophagic processes such as lipophagy and starch degradation in plants and animals, respectively, were not activated in the mutant despite autophagic induction. Thus, T411 cells have reduced survival because decreased ATP levels compromise essential cellular functioning (Johnson et al., 2014). Viability tests

on T411 and wild-type cells under acute and prolonged starvation and growth conditions revealed a progressive increase in T411 cell death in the prolonged growth and under chronic N starvation (Fig. 6, E and F). The down-regulation of *AMPK*, decreased ATP, and increased FFA levels in T411 suggest a positive interaction between PI3K with *AMPK* under starvation conditions, similar to what is observed in mammalian cells (Hardie et al., 2012). Moreover, our study supports recent studies that suggest that TAG and starch accumulation are essential processes for energy storage during stress and starvation. These processes are primarily aimed at survival of the organism and are interlinked to nutrient sensing (Couso et al., 2016; Juergens et al., 2016). Our study confirms that overflow of acetate toward TAG and starch is possible (Juergens et al., 2016). At the same time, overproduction of TAG and starch would be detrimental to the survival of the organism rather than a fitness benefit. Therefore, PI3K signaling, in combination with other regulatory networks involved in nutrient sensing, lipogenesis, and starch synthesis, are responsible for the fine balance of survival, fitness, and storage of energy molecules.

Based on the results of this and other studies, we propose that *AMPK* inhibits several critical genes in cellular signaling and metabolism, including *acetyl-CoA carboxylase* and *fatty acid synthase*, which are critical for fatty acid biosynthesis (Hardie et al., 2012; Couso et al., 2016; Juergens et al., 2016; Fig. 7). As PI3K KD resulted in *AMPK* down-regulation, enhanced FA biosynthesis was observed in the mutant (Fig. 7). The increased transcript abundance of key membrane lipid biosynthesis genes, down-regulation of *PKA*, and lipid profiling results in PI3K KD together reveal that PI3K influences membrane lipids levels by initiating membrane lipid hydrolysis. This might be achieved via the regulation of PKA levels, as in the case of adipocytes (Rambold et al., 2015). Therefore, regulation of PKA levels via inositide signaling is likely to have a major role in membrane lipid hydrolysis, which in turn leads to TAG overaccumulation as in the wild type. To date, no mutant showing highly reduced membrane lipid hydrolysis yet high TAG levels under stress or starvation has been reported. Thus, the inositide-induced regulatory mechanism behind the lipid turnover via PKA should be further explored.

Second, our results from the starch analysis in acute as well as prolonged starvation and growth indicate that starch levels in the PI3K KD tend to reduce in prolonged starvation, which is consistent with the transcriptomic results (Supplemental Fig. S4E; Fig. 5). The gene network analyses show that carbon flux goes toward glycolysis by down-regulation of key starch synthesis genes as well as up-regulation of several glycolysis genes in the PI3K KD. This trend is contrary to the recent results obtained from high starch mutants following gamma irradiation, which again highlights the role of PI3K signaling in starch and carbon metabolism (Koo et al., 2017).

Third, our results indicate that a majority of TCA cycle genes were highly downregulated in the mutant line (Fig. 5). The mutant line accumulates TAG by FA biosynthesis bypassing the TCA cycle through the down-regulation of key TCA cycle genes, including *PCK1* encoding phosphoenolpyruvate carboxykinase. *PCK1* in *C. reinhardtii* is acknowledged to be a lynchpin in gluconeogenesis and, in general, a cataplerotic and feeder enzyme for many downstream processes, including FA biosynthesis and lipid metabolism (Yang et al., 2009; Goodenough et al., 2014; Montal et al., 2015). Several studies in *C. reinhardtii* also emphasize the role of TCA cycle in lipid accumulation and carbon utilization (Plancke et al., 2014; Couso et al., 2016). In this study, transcriptomic and gene network analyses add further credence to the role of *PCK1* and the TCA cycle in the regulation of various processes related to carbon and energy metabolism as well as its regulation by PI3K signaling.

Lastly, our network analyses elucidate that genes involved in glycolysis were upregulated. In particular, those involved in the last two steps, *PGH1* and *PYK*, encoding Enolase or Phosphoenolpyruvate hydratase and Pyruvate kinase, respectively. In the case of *PYK*, four out of the five isozymes were upregulated, whereas the transcript abundance of the fifth isozyme (*PYK4*) could not be determined. In addition to the down-regulation of TCA cycle genes, the up-regulation of the gene encoding Pyruvate dehydrogenase, *PDC2*, involved in the conversion of pyruvate derived from glycolysis to acetyl-CoA, confirms the direction of carbon flux toward FA biosynthesis (Avidan et al., 2015). This result is contrary to the expression profile of wild type in this study, as well as in high starch strains obtained from gamma irradiation (Koo et al., 2017). These results, along with the up-regulation of most genes involved in the FA biosynthetic pathway and the levels of ATP and FFA in PI3K KD, suggest that the direction of carbon flux is toward FFA biosynthesis. However, the network analyses indicate expression levels of genes, while the direction of carbon fluxes have been presented based on the concurrence of network analyses with lipids, FFA, and ATP levels but devoid of respective enzymatic activities. Moreover, several inferences have been made with respect to animal and land plant models as *C. reinhardtii* is recognized to perform several animal and plant functions (Merchant et al., 2007), and the research on regulatory mechanisms in *C. reinhardtii* is still in its infancy.

Overall, highly reduced membrane lipid hydrolysis under stress increases the burden of TAG accumulation on FFA biosynthesis. Consequently, the T411 mutant line diverts carbon via enhanced glycolysis for FFA synthesis and bypasses the TCA cycle, which results in highly reduced ATP levels under prolonged starvation (Johnson and Alric, 2013; Johnson et al., 2014; Gargouri et al., 2015). Thus, PI3K regulates the fine homeostasis of membrane lipids to TAG, and without PI3K, TAG synthesis through continued FFA biosynthesis causes cytotoxicity, which may also explain the decreased viability of the PI3K KD (Li et al., 2012; Rambold et al., 2015). Cytotoxicity and reduced ATP generation dras-

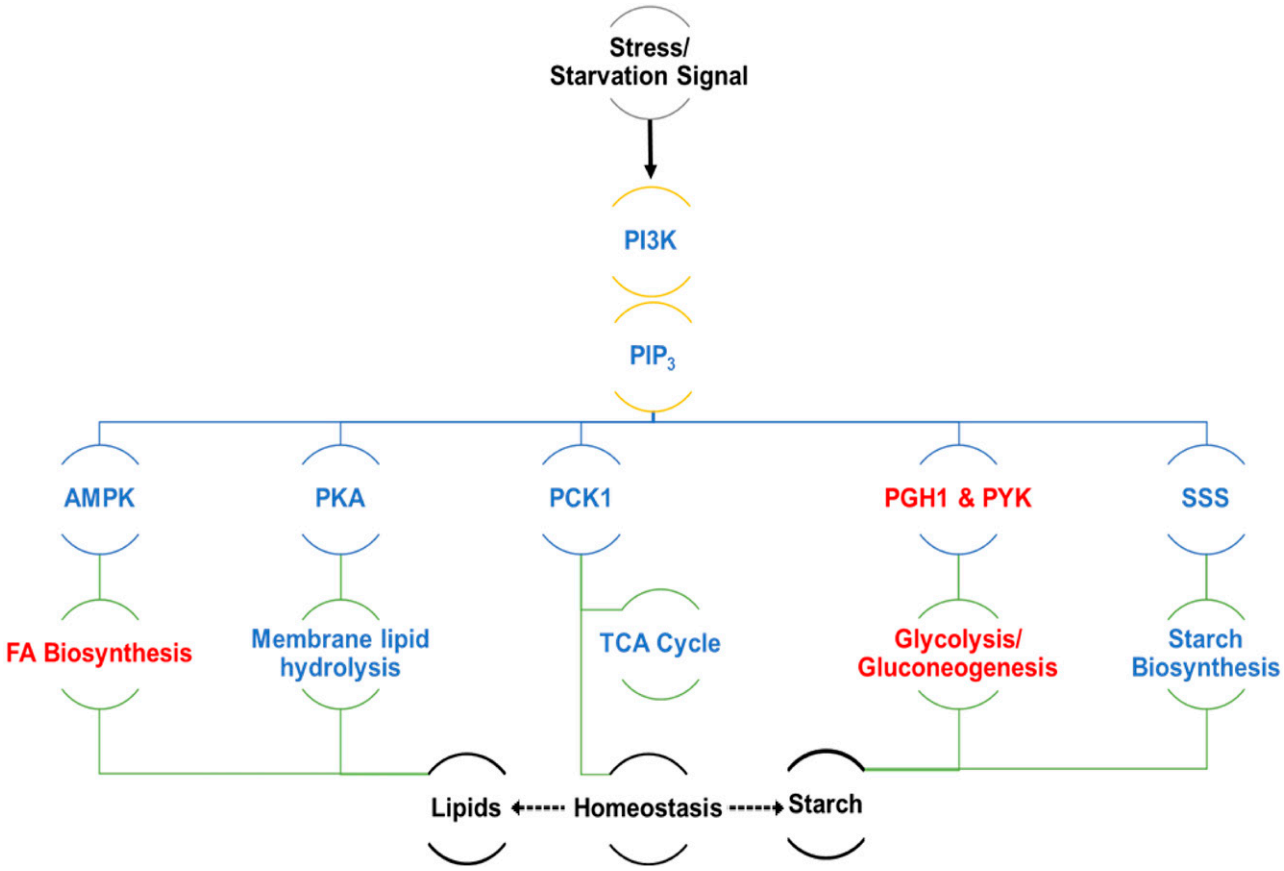

Figure 7. Proposed model of PI3K signaling network in algae under N starvation based on relative gene expression in T411 and its unique physiology. Changes in the relative mRNA levels of genes identified in the PI3K signaling pathway in T411 under –N conditions compared to wild-type cells grown in the same conditions. Genes and pathways denoted in blue are downregulated and those in red are upregulated in T411. In case of pathways, colors denote the response of the majority of genes. For detailed gene annotation, please refer to Supplemental Table S5.

tically reduce the likelihood of survival under stress conditions. Therefore, membrane lipid hydrolysis should be achieved for TAG synthesis and energy homeostasis in starvation condition (Fig. 7). Otherwise, as in the case of PI3K, TAGs need to be accumulated through FA biosynthesis, which is a highly energy-consuming process.

Taken together, these events result in drastic changes in cellular energetics in the PI3K KD (Williams and Laurens, 2010). Such a metabolism would drive higher biofuel yields in algae but compromise the effective survival strategy of high-ATP generation and reduced FFA and ROS generation under prolonged stress (Pérez-Pérez et al., 2012). Moreover, a recent study has pointed out that interactions occur between nutrient sensing by TOR kinase signaling and inositide signaling (Couso et al., 2016). Our study also proposes a possible interaction between TOR and PI3K signaling for nutrient sensing and growth. However, PI3K signaling is the likely controller of carbon flux toward TAG accumulation. Further studies are needed to ascertain the primacy of the PI3K signaling system over TOR or AMPK signaling, or vice versa (Couso et al., 2016).

Algal biofuel production is at a crossroads over low yields resulting from inadequate knowledge of basic mechanisms that drive TAG and starch accumulation. In this study, we show that class III PI3K, the oldest and the only class of PI3K in algae, mediates homeostasis of lipid, starch, FFA, and ATP. The main objective behind extensive carbon storage and partitioning in algae under stress and starvation is survival. PI3K signaling initiates this metabolic transformation as a response to oligotrophic environments encountered by algae. When this mechanism is compromised in the PI3K KD, the mutant eventually is relatively incompetent to survive under sustained nutrient-deficient condition compared to wild type. The excess FFA generated in the mutant even after prolonged starvation indicates similarities with tumor cells, but these FFA were not adequately quenched in the mutant, unlike the latter, affecting growth and survival. From a biofuel standpoint, the T411 line has higher lipid and starch

contents in acute starvation conditions, and therefore increased biofuels yield. This study is at the forefront of signal transduction pathway engineering in algae. Further progress would expand our understanding of the regulatory processes, augment productivity of desired algal biofuels, and enable faster commercialization.

The results of this study point to the existence of stable homeostasis between starch and lipid synthesis in algae, synthesis of which are prevalent in plant and animal models, respectively (Merchant et al., 2007). The PI3K signaling cascade in algae shows functions of animal PI3K signaling cascade as well as its plant counterpart, making algae a focal model to study fundamental and evolutionary aspects of lipid signaling cascade in eukaryotes.

MATERIALS AND METHODS

Strains, Mutants, Media, and Growth Measurements

The wild-type *Chlamydomonas reinhardtii* strain cc-124 (*137c nit1 NIT2 mt*$^{-}$) was obtained from the *Chlamydomonas* Resource Center (CRC) (http://chlamycollection.org/; MN University), and *sta6* (cw15 nit1 NIT2 arg7-7 sta6-1::ARG7 mt^{+}) was obtained from Prof. Ursula Goodenough. *Scenedesmus obliquus* NIES 2279 was also used in this study. *C. reinhardtii* strain cc-124 was used to generate the KD mutants using the amiRNA silencing method described previously (Molnar et al., 2009). Oligos were designed using the primer design function of WMD2, followed by ligation to pChlamiRNAint vector. The resultant vector was cloned in *Escherichia coli*, transformed in wild type and initially screened under the selective pressure of paromomycin (10 µg mL^{-1}). The sequences of oligos used for amiRNA knockdown are presented in Supplemental Table S3. The primers used for verifying the KD lines are presented in Supplemental Table S4. All three KD lines have been maintained for at least 4 years from the date of generation without any sign of change in the phenotypes. *C. reinhardtii* were grown in TAP medium at 25°C under continuous illumination of 100 µE m^{-2} s^{-1}, and 1,000 µE m^{-2} s^{-1} was used for the high-light condition. The cultures were grown until the late exponential phase with continuous shaking at 100 rpm (6 d). The cultures were centrifuged, washed with nitrogen-free TAP medium (TAP–N), and then resuspended at a cell concentration of 10^{6}/mL in TAP–N (N starvation; Ramanan et al., 2013). The cells were centrifuged at 3,000*g* in the early stationary phase (9 d, +N condition), acute starvation conditions (48 h, –N condition), prolonged growth (21 d, 21D+N) or starvation conditions (15 d, 15D–N), or at defined time intervals. The cells were grown until the late exponential phase and treated with inhibitors. For –N samples, the cells were immediately treated with inhibitors (Crespo et al., 2005). The cells were then collected at 24 h for image analysis or at defined time intervals. To ascertain the growth of cells (wild-type and KD lines) in mixotrophic and photoautotrophic modes in both +N and –N conditions, the cells were spotted in TAP agar plates after serial dilution and medium without acetate (Tris-minimal medium). The pH of the all the medium was adjusted using 1 N hydrochloric acid. The *S. obliquus* cells were grown in BG11 medium and treated with inhibitor in the late exponential phase (8 d) at the same concentration used for *C. reinhardtii*. The cells were collected at 24 h for image analysis or at defined time intervals. At least three biological replicates (three separate culture flasks with identical conditions) were used in all analyses. The cells were counted using a hemocytometer, and the dry cell weight was determined as described previously (Ramanan et al., 2013). The cell size and cell aspect ratio were calculated using optical microscopy fitted with live cell analytical software (Nikon; $n \geq 100$).

Lipid Analyses

The sample preparation and lipid profiling were performed as previously described (Kim et al., 2013b). In brief, lipid profiling was performed using electrospray ionization tandem mass spectrometry on a linear ion-trap mass spectrometer (LTQ-XL, Thermo Fisher Scientific) equipped with an automated nanoinfusion/nanospray source (Triversa NanoMate System, Advion). The ionization voltage and gas pressure were set to 1.4 kV and 0.4 psi, respectively, and the source was controlled by Chipsoft 8.3.1 software (Advion). All lipid samples were dissolved in 500 mL of methanol:chloroform mixture (9:1, v/v) containing 7.5 mM ammonium acetate. Five milliliters of the reconstituted lipid sample was infused using an Advion ESI chip with 5.5 mm ID emitter nozzles (Kim et al., 2013b). The total lipid content in the samples was determined using a previously described modified Bligh and Dyer method (Lee et al., 2010). TAG was qualitatively visualized by staining with 1 µg/mL BODIPY 505/515 (Invitrogen). The samples were incubated in the dark for 5 min and then imaged using confocal laser scanning microscopy merged with differential interference contrast micrographs (Carl Zeiss; Velmurugan et al., 2014). The TAG levels in the cells stained with BODIPY were quantified by FACS (Hyka et al., 2013; Velmurugan et al., 2014). The fluorescence intensity obtained from FACS analysis was normalized with chlorophyll autofluorescence and is presented as a ratio. The mutant and wild-type cells did not show any significant difference in chlorophyll content. The TAG levels were also quantified colorimetrically according to the manufacturer's protocol after chlorophyll extraction to prevent interference (ab65336; Abcam). The fatty acid methyl ester (FAME) profile of the samples was determined by gas chromatography fitted with a flame ionization detector (Shimadzu) using a 37-component FAME mix as the reference standard (Sigma-Aldrich; Lee et al., 2010).

RNA Isolation and Gene Expression Experiments

Total RNA was isolated from 10^{8} wild-type and mutant cells using an RNA isolation kit (Invitrogen). The cDNA synthesis was performed using GoScript reverse transcription kit for RT-qPCR (Promega) or as mentioned in the manufacturer protocol for RNA-seq (Illumina). The resulting libraries were sequenced using the Illumina HiSeq 2000 system and HiSeq 2500. The samples were normalized to 100 ng of total RNA prior to RT-qPCR. The *C. reinhardtii* beta subunit-like polypeptide (*CBLP*) gene was used as an endogenous control. The qPCR was performed using a Peltier Thermal Cycler with a Chromo4 detector (Bio-Rad Technologies) with the following reaction conditions: 95°C for 15 min, followed by 40 cycles of 95°C for 20 s, 66°C for 30 s, and 72°C for 20 s. The reaction was followed by melting curve analysis and then an extension of 5 min. The gene expression fold change was calculated using the $2^{-\Delta\Delta CT}$ method. The PCR and RT-qPCR primer sequences used in this study are presented in Supplemental Table S4.

Protein Isolation, Quantification, Enzyme Assay, and Immunoblot

The total protein extract was prepared using a plant total protein extraction kit with 10^{8} cells (PE0230, Sigma-Aldrich). The resulting protein concentration was estimated using Bradford reagent and a BSA standard (Sigma-Aldrich). The PI3K enzyme assay was performed as described in the manufacturer's protocol (K-3000, Echelon Biosciences). The immunoblot analysis was performed as described previously (Pérez-Pérez et al., 2010).

Starch and Chlorophyll Analyses

The starch analysis was performed using a starch (GO/P) assay kit (STA20; Sigma-Aldrich). The chlorophyll *a* concentration was determined as previously described using chlorophyll *a* from *Anacystis nidulans* as a standard (C6144; Sigma-Aldrich; Porra et al., 1989).

ATP, FFA, and Viability Measurements

The ATP and FFA levels in the cells were determined by the fluorimetric method according to the manufacturer's protocol with 10^{8} cells after chlorophyll extraction to prevent interference (ab83355 and ab65341, respectively; Abcam). The cell viability was determined by Evans blue staining (E_x 620 nm/E_m 680 nm) followed by confocal laser scanning microscopy. Evans blue has been used for studying microalgal viability as it is a nonpermeating dye in live cells. However, in case of plasma membrane damage resulting in cell death, dye stains the cytoplasm and nucleus blue (Crutchfield et al., 1999). The intensity of Evans blue fluorescence was quantified using FACS. The fluorescence intensity obtained from FACS analysis was normalized with chlorophyll autofluorescence and is presented as a ratio (Hyka et al., 2013; Velmurugan et al., 2014).

Phylogenetic, Statistical, and Bioinformatic Analyses

The amino acid sequences used to construct the phylogenetic tree were retrieved from National Center for Biotechnology Information (NCBI). The phylogenetic analyses were conducted using a maximum parsimony method and were constructed with MEGA 5.0. The branch points were tested for significance by bootstrapping with 1,000 replications (Tamura et al., 2007).

Statistical analyses of experimental results were computed using SPSS 18 (SPSS Inc.). All experimental analyses were performed with at least three biological replicates unless otherwise indicated, and the mean value and SD bars are presented. ANOVA and *t* test were performed to generate *P* values. To select a mutant for further experimental analyses, including lipidomics and RNA-seq, PCAs were performed based on various morphological, physiological, and genetic analyses, such as area and shape, total lipid content, TAG levels, and *VPS34* gene expression levels of KD lines, mock, and wild type in both +N and –N conditions. The data were converted into a common scale through Z-transformation so that the mean and variance corresponded to 0 and 1 (Cho et al., 2015).

The raw RNA-seq data obtained from the sequencer were processed for quality via the following four steps: (1) quality control was checked on 100-bp paired-end data using FastQC (version 0.11.3; Andrews, 2010). (2) Adaptor sequence was filtered by cutadapt (version 1.8.3; Martin, 2011) containing Illumina True-seq adaptor sequences. (3) Quality trimming was performed by Sickle (version 1.33; Joshi and Fass, 2011) with Phred Quality Score of 20 (i.e., the chances of a base being called incorrectly was 1 in 100 bases). (4) Reads below 40-bp length were removed and truncated at the position of the first N, following which clean reads were obtained. The reads remaining after those steps were aligned to the reference genome Creinhardtii_281_v5.5 (http://genome.jgi.doe.gov/pages/dynamicOrganismDownload.jsf?organism=Creinhardtii) using TopHat2 (version 2.0.12), a fast splice junction mapper for RNA-seq reads (Kim et al., 2013a) that aligns RNA-seq reads to reference genomes using the ultra high-throughput short read aligner Bowtie2. The TopHat aligner allowed up to 2 mismatches, 2 gaps, 20 multihits, and minimum 50 bp to maximum 500,000 bp intron length. All aligned reads were counted by htseq-count of HTSeq (version 0.6.1; Anders et al., 2015) with "intersection-nonempty" overlap resolution model (–m intersection-nonempty) for counting uniquely mapped reads in each gene, and without strand-specific assay (–s no). The gene annotation file (GTF) used for the alignment step was transformed to UCSC format for quantification of gene expression. After counting raw reads, the htseq-count results of each sample was merged into one count matrix.

The differential gene expression was analyzed with edgeR (version 3.13.2; Robinson et al., 2010), which is a Bioconductor package applied in R (version 3.2.2). The software was used to identify statistically significant differentially expressed genes. A convenient and well-established approximation for RNA-seq is the negative binomial distribution, which represents a natural extension of the Poisson distribution. By default, edgeR uses the number of mapped reads and estimates an additional normalization factor to account for sample-specific effects (e.g. diversity) (Robinson and Oshlack, 2010). These two factors are combined and used as an offset in the negative binomial model. The ratios of the size factors should approximately match the ratios of the library sizes. Each column of the count table can be divided by the corresponding size factor to yield the normalized count values, which can be scaled to give counts per million (cpm; Anders et al., 2013). We used only tags that had at least 1 cpm in at least half of the sample size to increase the statistical power of the differential expression analysis. Additionally, a low-read-count filter was applied to remove lowly expressed genes. The significant differentially expressed genes were selected using two thresholds of Benjamini-Hochberg adjusted *P* value < 0.05 and fold-change > 2 (absolute value of $\log_2 > 1$).

The gene annotation is based on *C. reinhardtii* v5.5 locus IDs downloaded from Phytozome 10.3 (http://phytozome.jgi.doe.gov). For the genes with no annotation available in Phytozome, a gene annotation was obtained from ALGAEpath (http://algaepath.itps.ncku.edu.tw/index.html) based on the KEGG ortholog (Zheng et al., 2014). The detailed gene annotation and RNA-seq data are presented in Supplemental Table S5 and Supplemental Data Set 2. To perform the pathway analysis, genes were mapped onto the KEGG pathway provided in ALGAEpath (http://algaepath.itps.ncku.edu.tw/index.html). The genes for respective pathways were also visualized using hierarchically clustered heat maps. The genes were displayed by Heatplus in the R package software and were clustered by the complete method. We used four pathways (TCA cycle, glycolysis, starch, and Suc metabolism and FA biosynthesis) for the network analysis. The gene networks were visualized in Cytoscape (version 3.2.1), which is an open source network visualization and analysis software platform (Shannon et al., 2003). The edge size was fixed by relative weight of cpm values with that of the WT+N control sample. Each node weight was based on the fold-change values of all genes used in the analysis after normalization.

Accession Numbers

The genetic information from this article can be found in the Phytozome database under the following accession numbers: *VPS34*, Cre01.g035500.v5.5; *ATG8*, Cre16.g689650.v5.5. The accession numbers of other genes and proteins from this study can be found in Supplemental Table S5 and Supplemental Data Set 2.

Supplemental Data

The following supplemental materials are available.

Supplemental Figure S1. Changes in TAG fluorescence (BODIPY 505/515) and lipid content in the presence of the PI3K inhibitor 3MA (3MA, 1 mM).

Supplemental Figure S2. Morphological, genotypic, and phenotypic analyses of PI3K KD transformants used for PCA analyses.

Supplemental Figure S3. TAG levels under high-light conditions in wild-type and T411 line.

Supplemental Figure S4. Statistical analyses of lipid profiling samples.

Supplemental Figure S5. Heat map and cluster analysis of the differential gene expression of genes involved in flagellar assembly in wild type and T411 under +N and –N conditions.

Supplemental Figure S6. Gene and protein expression analyses of autophagy-related proteins.

Supplemental Table S1. Lipid species identified in all sample groups used in the lipid profiling.

Supplemental Table S2. Ratio of the intensity of identified lipid species in samples.

Supplemental Table S3. Artificial microRNAs used for gene silencing in this study.

Supplemental Table S4. Primers used in this study.

Supplemental Table S5. The detailed gene annotation information for all RNA-seq-related data analysis.

Supplemental Data Set 1. Video depicting the mobility of wild-type and mock cells grown till early stationary phase, whereas the T411 line is nonmotile.

Supplemental Data Set 2. RNA-seq data for heat maps and network analyses.

ACKNOWLEDGMENTS

The study is dedicated to Dr. Hyun-Joon La, who passed away in his prime on February 13, 2016. His comments greatly helped in improving the manuscript. We thank Prof. Ursula Goodenough for kindly sharing starchless mutants and for constructive criticism of a part of this research study. We also thank Dr. Min-Sung Park for his helpful feedback on this study as well as Ms. Hyang Ran Yoon and Dr. Hyeon-woo Oh for their assistance with microscopy analyses.

Received March 22, 2018; accepted May 2, 2018; published May 16, 2018.

LITERATURE CITED

Anders S, McCarthy DJ, Chen Y, Okoniewski M, Smyth GK, Huber W, Robinson MD (2013) Count-based differential expression analysis of RNA sequencing data using R and Bioconductor. Nat Protoc **8**: 1765–1786

Anders S, Pyl PT, Huber W (2015) HTSeq—a Python framework to work with high-throughput sequencing data. Bioinformatics **31**: 166–169

Andrews S (2010) FastQC. A quality control tool for high throughput sequence data. http://www.bioinformatics.babraham.ac.uk/projects/fastqc/

Avidan O, Brandis A, Rogachev I, Pick U (2015) Enhanced acetyl-CoA production is associated with increased triglyceride accumulation in the green alga *Chlorella desiccata.* J Exp Bot **66**: 3725–3735

Boss WF, Im YJ (2012) Phosphoinositide signaling. Annu Rev Plant Biol **63**: 409–429

Chakraborty A, Koldobskiy MA, Bello NT, Maxwell M, Potter JJ, Juluri KR, Maag D, Kim S, Huang AS, Dailey MJ, (2010) Inositol pyrophosphates inhibit Akt signaling, thereby regulating insulin sensitivity and weight gain. Cell **143**: 897–910

Chapman KD, Dyer JM, Mullen RT (2012) Biogenesis and functions of lipid droplets in plants: thematic review series: lipid droplet synthesis and metabolism: from yeast to man. J Lipid Res **53**: 215–226

Cho D-H, Baek K-H, Ramanan R, Ahn C-Y, Ahn K-H, Yoon B-D, Oh H-M, Kim H-S (2015) Hydrocarbon pollution does not influence bacterial diversity as much as geographic location: a Korean case study. Int J Environ Sci Technol **12**: 1889–1898

Couso I, Evans B, Li J, Liu Y, Ma F, Diamond S, Allen DK, Umen JG (2016) Synergism between inositol polyphosphates and TOR kinase signaling in nutrient sensing, growth control and lipid metabolism in *Chlamydomonas.* Plant Cell **28**: 2026–2042

Crespo JL, Díaz-Troya S, Florencio FJ (2005) Inhibition of target of rapamycin signaling by rapamycin in the unicellular green alga *Chlamydomonas reinhardtii*. Plant Physiol **139**: 1736–1749

Crutchfield ALM, Diller KR, Brand JJ (1999) Cryopreservation of *Chlamydomonas reinhardtii* (Chlorophyta). Eur J Phycol **34**: 43–52

Díaz-Troya S, Pérez-Pérez ME, Florencio FJ, Crespo JL (2008) The role of TOR in autophagy regulation from yeast to plants and mammals. Autophagy **4**: 851–865

Finet C, Timme RE, Delwiche CF, Marlétaz F (2010) Multigene phylogeny of the green lineage reveals the origin and diversification of land plants. Curr Biol **20**: 2217–2222

Gargouri M, Park J-J, Holguin FO, Kim M-J, Wang H, Deshpande RR, Shachar-Hill Y, Hicks LM, Gang DR (2015) Identification of regulatory network hubs that control lipid metabolism in *Chlamydomonas reinhardtii.* J Exp Bot **66**: 4551–4566

Goodenough U, Blaby I, Casero D, Gallaher SD, Goodson C, Johnson S, Lee JH, Merchant SS, Pellegrini M, Roth R, (2014) The path to triacylglyceride obesity in the sta6 strain of *Chlamydomonas reinhardtii.* Eukaryot Cell **13**: 591–613

Hardie DG, Ross FA, Hawley SA (2012) AMPK: a nutrient and energy sensor that maintains energy homeostasis. Nat Rev Mol Cell Biol **13**: 251–262

Hou Q, Ufer G, Bartels D (2016) Lipid signalling in plant responses to abiotic stress. Plant Cell Environ **39**: 1029–1048

Hu Q, Sommerfeld M, Jarvis E, Ghirardi M, Posewitz M, Seibert M, Darzins A (2008) Microalgal triacylglycerols as feedstocks for biofuel production: perspectives and advances. Plant J **54**: 621–639

Hyka P, Lickova S, Přibyl P, Melzoch K, Kovar K (2013) Flow cytometry for the development of biotechnological processes with microalgae. Biotechnol Adv **31**: 2–16

Irvine RF (2016) A short history of inositol lipids. J Lipid Res **57**: 1987–1994

Irvine RF, Letcher AJ, Stephens LR, Musgrave A (1992) Inositol polyphosphate metabolism and inositol lipids in a green alga, *Chlamydomonas eugametos.* Biochem J **281**: 261–266

Johnson X, Alric J (2013) Central carbon metabolism and electron transport in *Chlamydomonas reinhardtii*: metabolic constraints for carbon partitioning between oil and starch. Eukaryot Cell **12**: 776–793

Johnson X, Steinbeck J, Dent RM, Takahashi H, Richaud P, Ozawa S, Houille-Vernes L, Petroutsos D, Rappaport F, Grossman AR, (2014) Proton gradient regulation 5-mediated cyclic electron flow under ATP- or redox-limited conditions: a study of ΔATpase pgr5 and ΔrbcL pgr5 mutants in the green alga *Chlamydomonas reinhardtii.* Plant Physiol **165**: 438–452

Joshi NA, Fass JN (2011). Sickle: A sliding-window, adaptive, quality-based trimming tool for FastQ files (version 1.33). https://github.com/najoshi/sickle

Juergens MT, Disbrow B, Shachar-Hill Y (2016) The relationship of triacylglycerol and starch accumulation to carbon and energy flows during nutrient deprivation in *Chlamydomonas reinhardtii*. Plant Physiol **171**: 2445–2457

Kajikawa M, Sawaragi Y, Shinkawa H, Yamano T, Ando A, Kato M, Hirono M, Sato N, Fukuzawa H (2015) Algal dual-specificity tyrosine phosphorylation-regulated kinase, triacylglycerol accumulation regulator1, regulates accumulation of triacylglycerol in nitrogen or sulfur deficiency. Plant Physiol **168**: 752–764

Kim D, Pertea G, Trapnell C, Pimentel H, Kelley R, Salzberg SL (2013a) TopHat**2**: accurate alignment of transcriptomes in the presence of insertions, deletions and gene fusions. Genome Biol **14**: R36

Kim S-H, Liu K-H, Lee S-Y, Hong S-J, Cho B-K, Lee H, Lee C-G, Choi H-K (2013b) Effects of light intensity and nitrogen starvation on glycerolipid, glycerophospholipid, and carotenoid composition in *Dunaliella tertiolecta* culture. PLoS One **8**: e72415

Koo KM, Jung S, Lee BS, Kim J-B, Jo YD, Choi H-I, Kang S-Y, Chung G-H, Jeong W-J, Ahn J-W (2017) The mechanism of starch over-accumulation in *Chlamydomonas reinhardtii* high-starch mutants identified by comparative transcriptome analysis. Front Microbiol **8**: 858

Lee J-Y, Yoo C, Jun S-Y, Ahn C-Y, Oh H-M (2010) Comparison of several methods for effective lipid extraction from microalgae. Bioresour Technol 101(Suppl 1): S75–S77

Li X, Moellering ER, Liu B, Johnny C, Fedewa M, Sears BB, Kuo M-H, Benning C (2012) A galactoglycerolipid lipase is required for triacylglycerol accumulation and survival following nitrogen deprivation in *Chlamydomonas reinhardtii.* Plant Cell **24**: 4670–4686

Martin M (2011) Cutadapt removes adapter sequences from high-throughput sequencing reads. EMBnet.journal**17**: 10–12

Merchant SS, Prochnik SE, Vallon O, Harris EH, Karpowicz SJ, Witman GB, Terry A, Salamov A, Fritz-Laylin LK, Maréchal-Drouard L, (2007) The *Chlamydomonas* genome reveals the evolution of key animal and plant functions. Science **318**: 245–250

Merchant SS, Kropat J, Liu B, Shaw J, Warakanont J (2012) TAG, you're it! *Chlamydomonas* as a reference organism for understanding algal triacylglycerol accumulation. Curr Opin Biotechnol **23**: 352–363

Mikami K (2014) Structural divergence and loss of phosphoinositide-specific phospholipase C signaling components during the evolution of the green plant lineage: implications from structural characteristics of algal components. Front Plant Sci **5**: 380

Miller R, Wu G, Deshpande RR, Vieler A, Gärtner K, Li X, Moellering ER, Zäuner S, Cornish AJ, Liu B, (2010) Changes in transcript abundance in *Chlamydomonas reinhardtii* following nitrogen deprivation predict diversion of metabolism. Plant Physiol **154**: 1737–1752

Molendijk AJ, Irvine RF (1998) Inositide signalling in *Chlamydomonas*: characterization of a phosphatidylinositol 3-kinase gene. Plant Mol Biol **37**: 53–66

Molnar A, Bassett A, Thuenemann E, Schwach F, Karkare S, Ossowski S, Weigel D, Baulcombe D (2009) Highly specific gene silencing by artificial microRNAs in the unicellular alga *Chlamydomonas reinhardtii.* Plant J **58**: 165–174

Montal ED, Dewi R, Bhalla K, Ou L, Hwang BJ, Ropell AE, Gordon C, Liu W-J, DeBerardinis RJ, Sudderth J, (2015) PEPCK coordinates the regulation of central carbon metabolism to promote cancer cell growth. Mol Cell **60**: 571–583

Munnik T, Irvine RF, Musgrave A (1994) Rapid turnover of phosphatidylinositol 3-phosphate in the green alga *Chlamydomonas eugametos*: signs of a phosphatidylinositide 3-kinase signalling pathway in lower plants? Biochem J **298**: 269–273

Nemazanyy I, Montagnac G, Russell RC, Morzyglod L, Burnol A-F, Guan K-L, Pende M, Panasyuk G (2015) Class III PI3K regulates organismal glucose homeostasis by providing negative feedback on hepatic insulin signalling. Nat Commun **6**: 8283

Pérez-Pérez ME, Florencio FJ, Crespo JL (2010) Inhibition of target of rapamycin signaling and stress activate autophagy in *Chlamydomonas reinhardtii.* Plant Physiol **152**: 1874–1888

Pérez-Pérez ME, Lemaire SD, Crespo JL (2012) Reactive oxygen species and autophagy in plants and algae. Plant Physiol **160**: 156–164

Plancke C, Vigeolas H, Höhner R, Roberty S, Emonds-Alt B, Larosa V, Willamme R, Duby F, Onga Dhali D, Thonart P, (2014) Lack of isocitrate lyase in *Chlamydomonas* leads to changes in carbon metabolism and in the response to oxidative stress under mixotrophic growth. Plant J **77**: 404–417

Porra R, Thompson W, Kriedemann P (1989) Determination of accurate extinction coefficients and simultaneous equations for assaying chlorophylls

a and b extracted with four different solvents: verification of the concentration of chlorophyll standards by atomic absorption spectroscopy. Biochim Biophys Acta **975**: 384–394

Ramanan R, Kim B-H, Cho D-H, Ko S-R, Oh H-M, Kim H-S (2013) Lipid droplet synthesis is limited by acetate availability in starchless mutant of *Chlamydomonas reinhardtii*. FEBS Lett **587**: 370–377

Rambold AS, Cohen S, Lippincott-Schwartz J (2015) Fatty acid trafficking in starved cells: regulation by lipid droplet lipolysis, autophagy, and mitochondrial fusion dynamics. Dev Cell **32**: 678–692

Robinson MD, Oshlack A (2010) A scaling normalization method for differential expression analysis of RNA-seq data. Genome Biol **11**: R25

Robinson MD, McCarthy DJ, Smyth GK (2010) edgeR: a Bioconductor package for differential expression analysis of digital gene expression data. Bioinformatics **26**: 139–140

Romero-Campero FJ, Perez-Hurtado I, Lucas-Reina E, Romero JM, Valverde F (2016) ChlamyNET: a *Chlamydomonas* gene co-expression network reveals global properties of the transcriptome and the early setup of key co-expression patterns in the green lineage. BMC Genomics **17**: 227

Schmollinger S, Mühlhaus T, Boyle NR, Blaby IK, Casero D, Mettler T, Moseley JL, Kropat J, Sommer F, Strenkert D, (2014) Nitrogen-sparing mechanisms in chlamydomonas affect the transcriptome, the proteome, and photosynthetic metabolism. Plant Cell **26**: 1410–1435

Shannon P, Markiel A, Ozier O, Baliga NS, Wang JT, Ramage D, Amin N, Schwikowski B, Ideker T (2003) Cytoscape: a software environment for integrated models of biomolecular interaction networks. Genome Res **13**: 2498–2504

Shanware NP, Bray K, Abraham RT (2013) The PI3K, metabolic, and autophagy networks: interactive partners in cellular health and disease. Annu Rev Pharmacol Toxicol **53**: 89–106

Sheehan J, Dunahay T, Benemann J, Roessler P (1998) Look back at the U.S. Department of Energy's aquatic species program: biodiesel from algae; close-out report. US Department of Energy.

Singh R, Kaushik S, Wang Y, Xiang Y, Novak I, Komatsu M, Tanaka K, Cuervo AM, Czaja MJ (2009) Autophagy regulates lipid metabolism. Nature **458**: 1131–1135

Tamura K, Dudley J, Nei M, Kumar S (2007) MEGA**4**: molecular evolutionary genetics analysis (MEGA) software version 4.0. Mol Biol Evol **24**: 1596–1599

Trentacoste EM, Shrestha RP, Smith SR, Glé C, Hartmann AC, Hildebrand M, Gerwick WH (2013) Metabolic engineering of lipid catabolism increases microalgal lipid accumulation without compromising growth. Proc Natl Acad Sci USA **110**: 19748–19753

Vanhaesebroeck B, Stephens L, Hawkins P (2012) PI3K signalling: the path to discovery and understanding. Nat Rev Mol Cell Biol **13**: 195–203

Velmurugan N, Sung M, Yim SS, Park MS, Yang JW, Jeong KJ (2014) Systematically programmed adaptive evolution reveals potential role of carbon and nitrogen pathways during lipid accumulation in *Chlamydomonas reinhardtii*. Biotechnol Biofuels **7**: 117

Wang Y, Yu B, Zhao J, Guo J, Li Y, Han S, Huang L, Du Y, Hong Y, Tang D, (2013) Autophagy contributes to leaf starch degradation. Plant Cell **25**: 1383–1399

Wijffels RH, Barbosa MJ (2010) An outlook on microalgal biofuels. Science **329**: 796–799

Williams PJlB, Laurens LML (2010) Microalgae as biodiesel & biomass feedstocks: review & analysis of the biochemistry, energetics & economics. Energy Environ Sci **3**: 554–590

Wymann MP, Schneiter R (2008) Lipid signalling in disease. Nat Rev Mol Cell Biol **9**: 162–176

Yang J, Kalhan SC, Hanson RW (2009) What is the metabolic role of phosphoenolpyruvate carboxykinase? J Biol Chem **284**: 27025–27029

Yoon K, Han D, Li Y, Sommerfeld M, Hu Q (2012) Phospholipid:diacylglycerol acyltransferase is a multifunctional enzyme involved in membrane lipid turnover and degradation while synthesizing triacylglycerol in the unicellular green microalga *Chlamydomonas reinhardtii*. Plant Cell **24**: 3708–3724

Zaidi N, Lupien L, Kuemmerle NB, Kinlaw WB, Swinnen JV, Smans K (2013) Lipogenesis and lipolysis: the pathways exploited by the cancer cells to acquire fatty acids. Prog Lipid Res **52**: 585–589

Zheng H-Q, Chiang-Hsieh Y-F, Chien C-H, Hsu B-KJ, Liu T-L, Chen C-NN, Chang W-C (2014) AlgaePath: comprehensive analysis of metabolic pathways using transcript abundance data from next-generation sequencing in green algae. BMC Genomics **15**: 196